TITLE: ***Disruption of Core Stress Granule Protein Aggregates Promotes CNS Axon Regeneration***

SUMMARY: *Inhibition of G3BP1 promotes CNS regeneration*

AUTHORS: Pabitra K. Sahoo[1,2*], Nick Hanovice[3], Patricia Ward[4], Manasi Agrawal[1,5], Terika P. Smith[1], HaoMin SiMa[4], Jennifer N. Dulin[6,7], Lauren S. Vaughn[1], Mark Tuszynski[6], Kristy Welshhans[1,9], Larry Benowitz[3], Arthur English[4], John D. Houle[8], Jeffery L. Twiss[1,9]

AFFILIATIONS:
[1] Department of Biological Sciences, University of South Carolina; Columbia, South Carolina USA.
[2] Department of Biological Sciences, Rutgers University – Newark; Newark, New Jersey USA.
[3] Boston Children's Hospital; Cambridge, Massachusetts USA.
[4] Department of Cell Biology, School of Medicine, Emory University; Atlanta, Georgia USA.
[5] Department of Biology, Kent State University; Kent, Ohio USA.
[6] Department of Neurosciences, University of California – San Diego; LA Jolla, California USA.
[7] Department of Biology, Texas A&M University; College Station, Texas USA.
[8] Department of Anatomy and Neurobiology, Drexel University College of Medicine; Philadelphia, USA.
[9] Carolina Autism and Neurodevelopment Research Center; University of South Carolina, Columbia, South Carolina, USA.

* Corresponding Author: Pabitra K Sahoo, Ph.D.
Department of Biological Sciences
Rutgers University Newark
225 University Avenue, LSC-601C
Newark, NJ 07102 USA
phone – 1-973-353-3493; email – pabitra.sahoo@rutgers.edu

ABSTRACT: Depletion or inhibition of core stress granule proteins, G3BP1 in mammals and TIAR-2 in *C. elegans*, increases axon regeneration in injured neurons that show spontaneous regeneration. Inhibition of G3BP1 by expression of its acidic or 'B-domain' accelerates axon regeneration after nerve injury bringing a potential therapeutic intervention to promote neural repair in the peripheral nervous system. Here, we asked if G3BP1 inhibition is a viable strategy to promote regeneration in the injured mammalian central nervous system where axons do not regenerate spontaneously. G3BP1 B-domain expression was found to promote axon regeneration in both the mammalian spinal cord and optic nerve. Moreover, a cell permeable peptide to a subregion of G3BP1's B-domain (rodent G3BP1 amino acids 190-208) accelerated axon regeneration after peripheral nerve injury and promoted the regrowth of reticulospinal axons into the distal transected spinal cord through a bridging peripheral nerve graft. The rodent and human G3BP1 peptides promoted axon growth from rodent and human neurons cultured on permissive substrates, and this function required alternating Glu/Asp-Pro repeats that impart a unique predicted tertiary structure. These studies point to G3BP1 granules as a critical impediment to CNS axon regeneration and indicate that G3BP1 granule disassembly represents a novel therapeutic strategy for promoting neural repair after CNS injury.

INTRODUCTION

Though the mammalian peripheral nervous system (PNS) can spontaneously regenerate injured axons, the growth rates are extremely slow at about 2 mm/day (*1*). Regenerating PNS axons can successfully navigate to their targets over short distances and restore at least partial function. However, PNS nerve regeneration for distances more than 5-6 cm is much less successful; this has been attributed to a progressive decline of the growth-supportive environment of the distal nerve and/or the receptivity of target tissues for reinnervation (*1*). Successful axon regeneration in the central nervous system (CNS) is even more problematic, as CNS neurons have a considerably lower intrinsic growth capacity than PNS neurons and the extracellular environment of the injured CNS actively inhibits axon regeneration (*2*). Thus, there are unmet clinical needs to accelerate PNS axon regeneration and to enable CNS axon regeneration.

Activation of the mTOR pathway, which increases overall cap-dependent protein synthesis, has been shown to promote axon regeneration in the injured CNS and PNS (*3-9*). Indeed, deletion of PTEN or inhibition that increases the activity of the mTOR pathway promotes regeneration of corticospinal tract axons in the injured spinal cord that are typically among the most refractory to regeneration (*7*). Protein synthesis in axons has been shown to facilitate PNS axon regeneration (*10*). Intra-axonal protein synthesis is a well-established mechanism in cultured CNS neurons, where the axon uses locally synthesized proteins for directional growth; there are now multiple lines of evidence indicating that many CNS neurons retain the capacity for intra-axonal protein synthesis well into adulthood (*11-13*), and some evidence for mRNA translation in spinal cord axons (*14-17*). We previously showed that intra-axonal RNA-protein granules containing the core stress granule protein G3BP1 slow PNS axon regeneration by sequestering mRNAs and attenuating their translation in injured axons (*18*). Stress granules that form by liquid-liquid phase separations (LLPS) are typically seen during metabolic or oxidative stress conditions and are used to store mRNAs encoding proteins that are not needed to

respond to the stress (*19*). However, axons use these as RNA storage depots in the apparent absence of any stress signals (*18, 20*), and disassembly of neuronal G3BP1 granules promotes intra-axonal protein synthesis and accelerates PNS axon regeneration (*18, 20*). Here, we asked whether inhibiting the RNA sequestration function of G3BP1 has therapeutic potential for promoting CNS axon regeneration.

RESULTS

G3BP1 granules attenuate axon regeneration in the central nervous system.

We previously showed that G3BP1 granules slow PNS axon regeneration and that expressing G3BP1's acidic domain or 'B-domain', consisting of rat G3BP1 amino acids 141-220 (UniProt ID: D3ZYS7_RAT), accelerates axon regeneration following sciatic nerve crush injury (*18*). G3BP1 B-domain expression decreases both the size and number of axonal G3BP1 granules, increases intra-axonal protein synthesis in cultured sensory neurons, and accelerates PNS nerve regeneration (*18*). Thus, the exogenously expressed G3BP1 B-domain acts as a 'dominant negative' agent. With these effects seen in PNS axons when G3BP1 is inhibited, we hypothesized that axonal G3BP1 granules could also affect the ability of CNS axons to regenerate.

Neural stem cells have been shown to promote CNS axon growth, where injured corticospinal motor axons can regrow to form a relay circuit across a site of spinal cord injury by forming synapses on stem cell-derived neurons grafted into the lesion site (*21, 22*). Lu *et al.* (2012) showed that neural progenitor cells isolated from the embryonic spinal cord ('caudalized grafts') promote growth of host corticospinal motor axons, whereas neural progenitor cells isolated from the embryonic telencephalon ('rostralized grafts') do not support regeneration into the graft (*21*). Using immunofluorescence for G3BP1 and TIA1, another core stress granule protein, we find that corticospinal axons in injured spinal cord contain more G3BP1-TIA1 stress granule-like aggregates in animals with a rostral graft, which does not support regeneration, than those with a caudal graft (**Fig. 1A**). This shows that spinal cord axons

contain G3BP1 and TIA1 granules, and that the presence of these intra-axonal stress granule-like aggregates relatively decreases the regeneration-promoting environment of a stem cell graft.

Axon growth from cultures of adult dorsal root ganglion (DRG) sensory neurons and embryonic cortical neurons from rats showed increased axon growth upon disassembly of G3BP1 granules induced by expression of the G3BP1 B-domain (*18*). To test the possibility that G3BP1 granules may contribute to the growth of adult CNS neurons, we asked whether B domain expression would alter rates of injured spinal cord axon growth within a permissive growth environment. For this, we transduced reticulospinal neurons using adeno-associated virus (AAV), serotype 5 expressing G3BP1 B-domain-blue fluorescent protein (BFP), full length G3BP1-BFP, or GFP. Fifteen days later, a C4 hemisection was performed and a peripheral nerve graft (PNG) was apposed to the rostral injury site adjacent to the reticulospinal tract as a growth-permissive environment (**Fig. 1B**). Immunofluorescence for axons performed at 20 days after spinal cord injury/PNG placement showed more axons extending further distances from the spinal cord/PNG apposition in the G3BP1 B-domain-BFP expressing animals compared to the G3BP1-BFP and GFP expressing animals (**Fig. 1C-D**). These data indicate that G3BP1 B-domain expression can promote adult CNS neuron axon growth *in vivo*.

The axons regenerating in the PNG above provide some similarities for spinal motor axons regenerating in peripheral nerve – *i.e.*, the reticulospinal neurons regenerated their axons through a growth-permissive PNS environment. Thus, we moved to an optic nerve injury model where CNS neurons must regenerate their axons through a growth-inhibitory CNS environment. For this, retinal ganglion cells (RGC) were transduced via intravitreal injection with AAV serotype 2 expressing G3BP1 B-domain-BFP, G3BP1-BFP, or GFP, and then crushed the optic nerve crush 14 days later (**Fig. 1E**). 14 days after optic nerve crush, immunofluorescent staining for growth associated protein 43 (GAP43) to detect regenerating axons and BFP/GFP to detect transduced neurons showed that G3BP1 B-domain expression in RGCs greatly increases axon regeneration (**Fig. 1F-G**). Interestingly, animals expressing the

G3BP1 B-domain appeared to show far higher number of axons proximal to the injury site (**Fig. 1F**). In contrast to many other CNS and PNS axotomies, optic nerve crush triggers death in the majority of RGCs (*23-26*), and we find that transduction with AAV2-G3BP1 B domain-BFP increased post-injury RGC survival compared to the two control conditions (**Extended Data Fig. 1**).

Expression of G3BP1 B-domain in PNS neurons disassembles axonal G3BP1 granules and in turn accelerates PNS nerve regeneration (*18*). To determine if expression of the G3BP1 B-domain affects G3BP1 granules in CNS axons, we compared G3BP1 granules in the reticulospinal axons in PNGs and RGC axons in the injured optic nerve using confocal microscopy where we could extract G3BP1 granule signals that overlapped with axonal markers across optical planes as a separate panel (projected XYZ images shown for 'Axonal G3BP1' panels in **Extended Data Fig. 2A and D**). G3BP1 B-domain expression in reticulospinal neurons and RGCs resulted in smaller and fewer G3BP1 granules in the axons compared to G3BP1 and control GFP expression (**Extended Data Fig. 2B-C and E-F**). Taken together, these findings indicate that expression of the G3BP1 B-domain can facilitate regeneration of injured CNS axons and overcome the growth-inhibitory environment of the injured CNS, likely through G3BP1 granule disassembly and release of axonal mRNAs for translation.

Cell permeable G3BP1 B-domain peptide increases PNS nerve regeneration.

Using synthetic cell-permeable peptides (CPP), we previously found that amino acids 147-166 and 190-208 of rat G3BP1 increase axon growth from cultured sensory and cortical neurons (*18*) whereas a cell permeable peptide (CPP) consisting of rat G3BP1 amino acids 168-189 had no significant effect (*18*). G3BP1 amino acid sequences for 147-166 and 190-208 CPPs are quite acidic with Glu or Asp residues occupying 11 of 21 (52.4%) and 8 of 19 residues (42.1%), respectively (**Fig. 2A**). The G3BP1 190-208 CPP was more effective than 147-166 CPP in our earlier study (*18*), so we tested whether the G3BP1 190-208 CPP might affect PNS axon regeneration *in vivo* using a clinically relevant paradigm where the CPP is applied after injury. For this, a mid-thigh sciatic nerve crush was performed on adult rats and 2

days later the G3BP1 190-208 or 168-189 CPP was injected just proximal to the injury site to achieve an estimated 113 µM concentration within the perineurium (**Fig. 2B**). G3BP1 190-208 CPP-injected animals showed a strong increase in axon regeneration at 7 days post-injury (5 days after peptide treatment) compared to G3BP1 168-189 CPP-injected animals, an effect that was particularly evident at longer distances down the nerve (**Fig. 2C-D**). The G3BP1 168-189 CPP-injected animals showed no significant difference from those injected with an equivalent volume of the vehicle control (phosphate-buffered saline [PBS]; **Fig. 2D**).

To determine if the accelerated nerve regeneration seen with the G3BP1 190-208 CPP brings functional improvements, we compared neuromuscular junction (NMJ) reinnervation in G3BP1 168-189 vs. 190-208 CPP-treated animals using compound muscle action potentials (CMAP) for the lateral gastrocnemius (LG) and tibialis anterior (TA) muscles (**Fig. 2B**). Recovery of CMAPs was significantly accelerated in the animals treated with G3BP1 190-208 CPP treatment for both the LG and TA at 2 and 4 weeks after sciatic nerve crush (**Fig. 2E, Extended Data Fig. 3A**). There were no differences between the G3BP1 190-208 and 168-189 CPP-treated animals at 8 weeks post-injury (**Fig. 2E**), consistent with spontaneous regeneration in the PNS; similar results were previously reported for sciatic nerve crush recovery in AAV-G3BP1 B-domain transduced animals (*18*). It should be noted that significant differences between the G3BP1 190-208 and 168-189 CPP-treated animals were also not seen at 6 weeks post-injury, which points to a limited *in vivo* duration for the G3BP1 190-208 CPP activity and emphasizes an opportunity to improve peptide stability.

The G3BP1 190-208 sequence contains seven Glu-Pro (EP_7) repeats flanked by N-terminal Val-Val and C-terminal Val-Ser-Asp (**Fig. 2A**). We sought to determine critical residues for function of the 190-208 G3BP1 CPP by asking whether sequence alterations modified its axon growth-promoting activity in adult DRGs cultured on laminin. We initially tested 190-208 G3BP1 CPP from a different vendor ('Bachem') and got identical results to the previous synthetic peptide (**Fig. 2F, Extended Data Fig**

3B-D), and a modified 190-208 CPP in which all Glu residues in the EP_7 region were replaced with similarly acidic Asp residues promoted axon growth to a similar extent as the original 190-208 CPP (**Fig. 2F, Extended Data Fig. 3B-D**). Similarly, removing the N- and C-terminal residues flanking the EP_7 repeats (G3BP1 192-205 CPP) maintained full axon growth-promoting activity (**Fig. 2F, Extended Data Fig. 3B-D**), indicating that just the seven EP repeats are sufficient to promote axon growth. However, a scrambled 190-208 G3BP1 CPP where the EP_7 was changed to seven Glu followed by seven Pro (E_7P_7) generated axon lengths that were not significantly different than the non-functional 168-189 G3BP1 CPP (**Fig. 2F, Extended Data Fig. 3B-D**). Taken together, these data indicate that axon growth-promoting functions of the 190-208 G3BP1 CPP require alternating acidic residues with Pro.

The G3BP1 147-166 sequence bears some similarities to the 190-208 sequence with a preponderance of Glu residues (**Fig. 2A**). Interestingly, we have shown that Casein kinase 2 alpha (CK2α)-dependent phosphorylation of G3BP1 on Ser 149 ($G3BP1^{PS149}$) causes G3BP1 granule disassembly and decreases G3BP1's RNA binding activity (*20*). Considering the functional effects of Ser 149 phosphorylation, we asked whether replacing Ser 149 with an acidic residue to mimic phosphorylated G3BP1 ($147\text{-}177^{S149E}$) would increase the axon growth effects of G3BP1 147-166 CPP to levels comparable to the G3BP1 190-208 CPP. G3BP1 $147\text{-}149^{S149E}$ CPP treatment generated axon lengths intermediate between the G3BP1 168-189 and G3BP1 190-208 CPPs (**Fig. 2F, Extended Data Fig. 3B-D**), indicating that the S149E modification did not increase efficacy of the 147-166 CPP. We further tested a CPP containing the human G3BP1 sequence corresponding to rat amino acids 190-208 (human 191-209). The human 191-209 CPP promoted axon growth comparable to the rat 190-208 CPP despite an Asp at residue 197 (instead of Glu) and Gln at residue 204 (instead of Pro) within the EP_7 region (**Fig. 2A and F, Extended Data Fig. 3B-D**). Rat 190-208, rat 192-205 (EP_7), and human 191-209 CPPs also substantially increased neurite growth from glutamatergic neurons derived from human induced pluripotent stem cells (hiPSC) (**Fig. 2G, Extended Data Fig. 4**).

Axon branching in adult DRG cultures treated with the G3BP1 CPP variants was also assessed. The rat 192-205, human 191-209, and rat 147-166^{S149E} G3BP1 CPPs increased branch density by ~12% as compared to the rat 190-208 and other CPP variants, which were not different than the rat 168-189 CPP with no axon outgrowth effects (**Extended Data Fig. 3D**). Similarly, rat 192-205 and human 191-209 G3BP1 CPPs increased neurite branch density in the hiPSC-derived neurons, but the rat 190-208 and scrambled 190-208 G3BP1 CPPs were no different than the rat 168-189 CPP (**Extended Data Fig. 4C**). Notably, each of the CPPs that increased the total axon/neurite length also increased the length of the longest axon/neurite per neuron (**Extended Data Figs. 3C and 4B)**, indicating that the increased branching seen with rat 192-205 and human 191-209 CPPs do not account for the difference in total axon/neurite lengths shown above. In contrast, the increase in DRG total axon length and longest axon per neuron induced by the rat 147-166^{S149E} CPP was modest with non-significant Z score compared to the population mean, suggesting that it had minimal effects on elongating axon growth (**Fig. 2F, Extended Data Fig. 3C-D**).

G3BP1 190-208 cell-permeable peptide differentially alters CNS axon regeneration depending on the local environment.

Since the G3BP1 190-208 CPP successfully promotes PNS axon regeneration (**Fig. 2B-E**) and the G3BP1 B-domain promotes regeneration of reticulospinal axons (**Fig. 1B-D**), we asked whether this CPP strategy might also be effective in promoting CNS axon regeneration. To test this, we performed a C4 hemisection with PNG apposed close to the rostral injury site for reticulospinal axon growth (**Fig. 3A**). The same day, the rat 168-189 or 190-208 G3BP1 CPPs were injected directly into the spinal cord just rostral to the injury site and regeneration through the PNG was evaluated 10 days after injury by immunostaining for axonal markers (**Fig. 3A**). Increases in axon profile numbers were only seen for the rat 190-208 compared to 168-189 G3BP1 CPP-treated animals at the most proximal segment of the PNG (**Fig. 3B**). Thus, in contrast to the effect of the G3BP1 B-domain in this experimental model, there were

no differences between treatment groups in the more distal segments (2-6 mm; **Fig. 3B**). Confocal microscopy for XYZ imaging of the proximal PNG segment was used to reconstruct the path and branches of individual regenerating reticulospinal axons across optical planes representing cross sections of the PNG in combination with *Neurolucida* software neurite tracking/branching function. Surprisingly, the 190-208 G3BP1 CPP-treated animals showed a remarkable increase in axon branching complexity in the proximal PNG compared to the 168-189 CPP-treated animals (**Fig. 3C-D**). Thus, although the 190-208 G3BP1 CPP increases reticulospinal outgrowth in PNGs, this appears to result in axon branching or sprouting rather than the axon elongation seen in PNGs with AAV-G3BP1 B-domain transduced reticulospinal neurons.

In the above spinal cord injury experiment, the CPPs were presented to axons directly in the injured spinal cord but the nerve regeneration experiments in Figure 2 presented the CPPs to axons in the permissive environment of the peripheral nerve. Thus, we asked if exposing regenerating reticulospinal axons to G3BP1 CPPs within the PNG might alter their growth differently. For this, we performed a C4 hemisection with descending PNG as in Figure 1; 30 days later, CPPs were injected into the distal PNG that was then apposed to the caudal spinal cord adjacent to the caudal injury site (**Fig. 3E**). Animals were euthanized 22 days later (52 days post-injury, 22 days CPP exposure) and spinal cords with attached PNG were analyzed for axon regeneration using SCG10 immunostaining. The 190-208 G3PB1 CPP-treated animals showed increased numbers of axons entering into the spinal cord from the PNG, and those axons extended considerably greater distances into the spinal cord compared to scrambled 190-208 CPP-treated animals (**Fig. 3F-G**). Thus, the 190-208 G3BP1 CPP can promote growth of injured adult spinal cord axons, but our data suggest that it generates different growth morphologies depending on whether the CPP is presented in the growth-inhibitory environment of the spinal cord or the growth-permissive environment of the PNG. We followed this observation up with a study of

animals that received an injection of 190-208 G3BP1 CPP only into the distal site of PNG apposition and found no enhanced axonal outgrowth under this condition (data not shown).

Axonal growth morphology induced by G3BP1 190-208 cell permeable peptide depends on growth environments.

To directly test the possibility that the G3BP1 190-208 CPP differentially alters axon growth depending on the permissiveness of the growth substrate, we evaluated neurite growth from embryonic day 18 (E18) rat cortical neurons cultured on growth-permissive (poly-D-lysine [PDL]) or growth-inhibitory (PDL + aggrecan) substrates. For neurons cultured on PDL, rat 190-208 G3BP1 CPP nearly doubled total axon length and distance the axon extended from the soma, had a smaller but significant effect on dendrite lengths, and decreased axon and dendrite branching compared to 168-189 CPP (**Fig. 4A, Extended Data Fig. 5**). In contrast, 190-208 G3BP1 CPP-treated cortical neurons cultured on PDL + aggrecan showed increased axon and dendrite branching compared to 168-198 CPP-treated neurons (**Fig. 4B**). Total axon and dendrite lengths were increased by 25% and 80%, respectively, for the 190-208 G3BP1 CPP-treated compared to 168-198 CPP-treated cortical neurons cultured on PDL + aggrecan; distance extended from the soma was not changed for the axons but was increased for the dendrites in these CNS neurons (**Fig. 4B, Extended Data Fig. 5B**). We had previously shown that G3BP1 190-208 CPP treatment increases axon lengths for DRG neurons grown on laminin (*18*). In contrast to the cortical neurons used above, DRG neurons only extend $Tau^{+}/MAP2^{-}$ neurites with other axonal features (*27-29*) in culture, so only axon growth can be evaluated in these cells. 190-208 G3BP1 CPP-treated DRG cultures showed increased axon lengths on laminin + aggrecan, but axon branching was also significantly increased compared to the 168-189 CPP-treated neurons (**Extended Data Fig. 5C-D**). Taken together, these data indicate that disassembling axonal G3BP1 granules using the 190-208 G3BP1 CPP in non-

permissive growth environments increases neurite branching, while the CPP promotes elongating axon growth in permissive growth environments.

Axon growth-inhibiting vs. -promoting substrates are known to differentially regulate activities of the small GTPases RhoA, Rac, and CDC42 (*30-34*). CSPGs, in particular, activate RhoA in distal axons, which promotes actin filament disassembly and growth cone retraction (*2*), and accordingly, inhibition of RhoA allows axons to grow on this non-permissive substrate (*35-37*). In contrast, axon growth-promoting stimuli (*e.g.*, neurotrophins) activate Rac and CDC42 in distal axons, which promotes actin filament assembly and growth cone advance (*34*). To determine if RhoA plays any role in the increased axon branching seen with rat 190-208 G3BP1 CPP treatment for neurons grown on the CSPG aggrecan, we pharmacologically inhibited RhoA in E18 rat cortical neurons cultured on PDL + aggrecan simultaneously with CPP treatment. For the control CPP-treated neurons (scrambled 190-208 G3BP1), RhoA inhibition increased total axon length/neuron but this is attributed in part to an approximately five-fold increase in axon branching compared to vehicle-treated neurons (DMSO; **Fig. 4C-D, Extended Data Fig. 5E**). For the rat 190-208 G3BP1 CPP-treated neurons, RhoA inhibition increased total axon length but decreased axon branching compared to DMSO-treated cultures (**Fig. 4D, Extended Data Fig. 5E**). Together, these data indicate that RhoA activity drives axon branching on the growth-inhibitory substrate when G3BP1 granules are inhibited. This raises the interesting possibility that intra-axonal signaling, driven by the permissiveness vs. non-permissiveness of the axon's environment, can shift the elongating morphology of CNS axon growth depending upon RhoA activity and G3BP1 granule formation status.

DISCUSSION

In contrast to the PNS, mature CNS neurons have a low capacity for axon growth after injury; this, plus the extracellular milieu of the injured brain and spinal cord, limits axon regeneration after traumatic CNS injuries (*2*). Consequently, interventions are needed to coax CNS axons to regenerate.

PNS axons can spontaneously regenerate but grow very slowly at 2-4 mm per day (*1*). We previously showed that decreasing LLPS of RNA-protein granules containing the core stress granule protein G3BP1 accelerates the regeneration of injured PNS axons (*18, 20*). Here, we show that expression of G3BP1's conserved B-domain (amino acids 141-220) accelerates regeneration of reticulospinal axons in the growth-permissive environment of a peripheral nerve grafted into the hemisected spinal cord and is sufficient to enable injured RGCs to regenerate axons in the growth-inhibitory CNS environment of the injured optic nerve. We previously found that this B-domain functions as a dominant negative agent by preventing axonal G3BP1 granule assembly and increasing axonal protein synthesis (*18*). Since G3BP1 B-domain expression in reticulospinal neurons and RGCs decreased granule formation by endogenous G3BP1 in their axons, G3BP1 B-domain expression in the CNS neurons likely increases regeneration by releasing axonal mRNAs encoding regeneration-associated proteins that are normally sequestered in G3BP1 granules. Notably, depletion of the *C. elegans* orthologue of TIA1, TIAR-2, similarly increased regeneration following axotomy by decreasing RNA-protein granules and increasing axonal protein synthesis (*38*). Together with the findings herein, this observation emphasizes that mRNA sequestration impedes mammalian CNS axon regeneration just as previously shown for a mammalian PNS nerve and for invertebrate axon regeneration (*18, 38*).

Some interventions that increase PNS axon regeneration have proven successful for promoting CNS axon regrowth, though this is often limited in terms of the extent of growth promotion. For example, conditioning lumbosacral sensory neurons by sciatic nerve crush injury accelerates axon regeneration after subsequent PNS injury and brings a degree of axon regrowth after dorsal column lesion in the spinal cord (*39*). This phenomenon is attributable to the entry of inflammatory cells into the injured PNS, which elevates levels of cell-derived growth factors including oncomodulin and SDF-1 (*40*). The PTEN→mTOR pathway has been manipulated to increase CNS and PNS axon regeneration either by attenuating PTEN activity or downstream interventions that more directly increase mTOR

activity (*4, 7*). PTEN activity can modify gene transcription (*41*), however, the increase in mTOR activation with PTEN deletion also converges on the translation machinery to globally increase cap-dependent protein synthesis (*42*). The resulting activation of the mTOR pathway can promote axon regeneration even in injured corticospinal tract axons that normally show very poor growth (*8*). *mTor* mRNA is locally translated in PNS axons in response to an injury-induced increase in axoplasmic Ca^{2+} (*20, 43*). This increase in axonal mTOR protein supports neuronal survival after injury (*43*) but is also needed for subsequent translation of axonal *Csnk2a1* mRNA, with newly generated CK2α phosphorylating G3BP1 and triggering G3BP1 granule disassembly to increase axonal protein synthesis (*20*). *mTor* mRNA is also locally translated in axons of cultured cortical neurons (*44*) and the mRNA and protein are present in growth cones of developing CNS neurons *in vivo* (*45*). In contrast to PNS and other CNS neurons, a large proportion of RGCs die after optic nerve injury; similar to what we show with G3BP1 B-domain expression in RGCs, deletion of the murine *PTEN* gene was shown to increase survival of axotomized RGCs in addition to promoting regeneration (*9*). Thus, it is highly likely that convergent mechanisms promote regeneration after mTOR pathway activation and G3BP1 granule disassembly with both promoting translation of localized mRNAs.

Though we have previously shown that G3BP1 B-domain and 190-208 CPP decrease axonal G3BP1 granules and promote translation of protein products that promote axon growth (*18*), it is not yet clear how either disrupts the G3BP1 granules. The B-domain is one of G3BP1's three intrinsically disordered regions (IDR) and is required for LLPS by G3BP1 (*46*). This region is well-conserved across vertebrate species, with mouse showing more than 85% homology to human, 67% to xenopus, and 46% to zebrafish based on G3BP1 sequences available in UniProt (*47*). The rodent 190-208 and human 191-209 sequences lie within G3BP1's IDR1, which intramolecularly interacts with the protein's IDR3 (*46, 48*). CPPs have been employed to disrupt protein-protein interactions (*49*). For example, CPPs were used to disrupt mutant Huntingtin's (HTT) protein-protein interactions in a Huntington disease model and DJ-1's

(PARK7) interactions in a Parkinson disease model (*50, 51*). Though the G3BP1 B-domain (IDR1) was shown to intramolecularly interact with the protein's IDR3 (*46, 48*), we do not detect coprecipitation of G3BP1 with a biotinylated 190-208 G3BP1 CPP, even when testing recombinant G3BP1 combined with crosslinking (data not shown). Thus, interruption of G3BP1's intramolecular interactions or interactions of multiple G3BP1 proteins with one another is an unlikely mechanism. G3BP1 is a core stress granule protein that we previously showed interacts with other stress granule proteins in PNS sensory axons including TIA1, although TIA1-only granules were also identified along axons that were not disrupted by the 190-208 G3BP1 CPP (*18*). Axonal G3BP1 colocalizes with TDP43, and rodent 190-208 G3BP1 CPP triggers disassembly of pathological TDP43 aggregates in axons of iPSC-derived human motor neurons (*52*). Depletion and knockout approaches have defined several core stress granule proteins and proximity biotinylation approaches have uncovered many G3BP1 interacting proteins (*46, 48, 53-55*). Additionally, G3BP1 binds to the adapter protein Anexin A11, which allows the RNP complex to be transported along axons by hitchhiking on lysosomes/endosomes as a means for delivering mRNAs into axons (*56*). Since we see that sustained exposure to the 190-208 G3BP1 CPP facilitates axon growth and delivery of new mRNAs into axons is needed for regeneration (*10*), the 190-208 CPP likely does not interrupt G3BP1-AnexinA11 interactions. Additional studies beyond the structure-activity studies included here will be needed to uncover how the G3BP1 CPP and B-domain disrupt G3BP1 granules.

The rodent 190-208 G3BP1 CPP contains seven Glu-Pro repeats, and a CPP with just the seven Glu-Pro repeats (rodent G3BP1 amino acids 192-205) is sufficient for neurite growth-promoting activity. Acidic residues with alternating prolines are essential for this growth promotion, because a CPP with Asp residues replacing Glu has full activity but its activity is lost on scrambling the Glu-Pro repeats. Tertiary structures of rodent 190-208 and human 191-209 G3BP1 sequences generated with *Pepfold3* (*57-59*) predict a kink in the peptide backbone at each Pro with the acidic side chains of each acidic residue projecting peripherally from the backbone (**Extended Data Fig. 3Ei-ii**), which is lost in the scrambled

rodent 190-208 G3BP1 CPP (**Extended Data Fig. 3Eiii**). These predicted 3D structure differences between rodent 190-208 and human 191-209 G3BP1 CPPs compared to scrambled rodent 190-208 CPP, as well as the rodent 147-168^{S149E} G3BP1 CPP (**Extended Data Fig. 3Eiv**), may contribute to differences in their growth promoting abilities.

It is intriguing that the 190-208 peptide increased branching of axons in the PNGs when presented in the non-permissive environment of the injured spinal cord (**Fig. 3A-D**) and for primary neurons cultured on non-permissive CSPG substrate compared to elongating growth on permissive laminin substrate (**Fig. 4B, Extended Data Fig 5A-D**). This effect is in contrast to G3BP1 B-domain expression that must begin before injury – this may point to different mechanisms underlying prevention of G3BP1 granule formation (i.e., viral-based B-domain expression before injury) vs. disassembly of formed G3BP1 granules (i.e., 190-208 G3BP1 CPP administration after injury). Interestingly, inhibition of RhoA partially reversed the increased branching seen in the 190-208 G3BP1 CPP-treated neurons grown on aggrecan (**Fig. 4C-D, Extended Data Fig 5E**). Activation of RhoA causes actin filament disassembly (*60*), and *RhoA* mRNA is locally translated in axons (*61*) with previous studies showed that CSPGs stimulate axonal *RhoA* mRNA translation in axons (*31*). This raises the possibility that the axon's environment determines either the complement of mRNAs released from G3BP1 granules or which released mRNAs are translated in the axons. *RhoA* mRNA has been detected in G3BP1-RNA coimmunoprecipitations (*62*). Axon branching requires local reorganization of the cytoskeleton (*63*), which increasing RhoA locally could support by disassembling actin microfilaments. CSPG stimulation can increase axoplasmic Ca^{2+} (*64, 65*) and axoplasmic Ca^{2+} levels can determine which axonal RNAs released from G3BP1 granules are translated through the phosphorylation of the translation factor eIF2α in axons (*20*). Interestingly, RhoA activation was shown to increase formation of TIA1- and FMRP-containing stress granules in other cellular systems (*66*), and CSPG-stimulated RhoA can activate the cytoplasmic histone deacetylase HDAC6 in distal axons (*65*). Deacetylation of G3BP1 lysine

376 by HDAC6 promotes G3BP1 granule assembly (*67*). Considering that the rat 190-208 G3BP1 and human 191-208 sequences do not include the post-translationally modified Ser 149 or Lys 376, we suspect that these CPPs do not alter post-translational modifications of G3BP1. Taken together, our data raise the possibility that successful long-distance CNS axon regeneration with G3BP1 granule inhibition will require simultaneous inhibition of RhoA.

In summary, our findings show that G3BP1 granules contribute to failed axon regeneration after optic nerve and spinal cord injury. Thus, disassembly of G3BP1 granules, as we have done here using G3BP1 B-domain expression or the 190-208 G3BP1 CPP, could bring a new strategy to promote neural repair following brain and spinal cord injuries, either on their own or strategically combined with other interventions. Importantly, the G3BP1 190-208 CPP strategy used here is effective when delivered after 2 days after PNS injury and 14 days after spinal cord transection, which elevates the potential clinical relevance of these reagents for neural repair treatments. Structure-activity relationship studies point to alternating acidic residue (Glu or Asp) and Pro repeats as the functional component of the 190-208 G3BP1 CPP. This presents opportunities for further refinement of the CPP activity, and since the 191-209 human G3BP1 CPP promotes axon growth in human iPSC-derived CNS neurons, we anticipate that similar reagents may have high translation value for neural repair in human patients.

MATERIALS AND METHODS

Animal use **–** Institutional Animal Care and Use Committees of University of South Carolina, Boston Children's Hospital, Emory University, University of California San Diego, Texas A&M University, and Drexel University approved all animal procedures. Sprague Dawley rats (SD; 175-250 g) were used for sciatic nerve injury, and spinal cord injury, and wild type 129s mice were used for optic nerve injury experiments. Survival surgery methods are described below.

Peripheral nerve injury **–** For crush injury of sciatic nerve, anesthetized rats or mice were subjected to a manual crush at mid-thigh two times at 15 sec each using fine jeweler's forceps as described (*68*). For *in vivo* cell permeable peptide (CPP) injections, 1 µl of 1 mM cell permeable peptides (diluted in 10 µl phosphate-buffered saline; PBS) were injected into sciatic nerves proximal to the crush site 2 days after injury. Concentration for *in vivo* peptide delivery into the nerve was determined based on estimated volume of a 1.5 mm nerve cylinder and diffusion of 2.5 mm in each direction giving a nerve volume of 8.84 mm^3. 10 µl solutions from above were injected in 3 different sites (~3.3 µl in each site) within 500 µm proximal to the injury site using Hamilton syringes to approximate an in vivo peptide concentration of 113 µM. The needle tip was inserted horizontally for 2-3 mm into the sciatic nerve for peptide injection over a 1-2 min period.

Analysis of muscle reinnervation after peripheral nerve injury **–** Following nerve injury and CPP injections, the extent of reinnervation of the hindlimb muscles was evaluated using in vivo electromyography (EMG). Anesthesia was induced with 5% isoflurane in 1 L/min oxygen and maintained at 2% isoflurane in 1 L/min oxygen.

Bipolar fine wire EMG electrodes were constructed from insulated nichrome wire (A-M Systems, Sequim, WA). The insulation over the distal 1 mm of the tips was removed by scraping with a scalpel blade and the tips of the two wires were staggered by 1 mm. Electrodes were then placed into the mid-belly of the lateral head of the gastrocnemius (LG) and tibialis anterior (TA) muscles using a 25 Ga

hypodermic needle. Once in place, the needle was removed and the wires were connected to the differential amplifiers. To stimulate the sciatic nerve, a small skin incision was made just inferior to the ischial tuberosity, exposing the sciatic nerve as it passes between the gluteal and hamstring muscles and proximal to the crush injury site. Two unipolar needle electrodes (Neuroline monopolar, 28 Ga; Ambu/AS, Columbia, MD) were placed on either side of the sciatic nerve, separated from each other by approximately 1 mm. Lead wires from the needles were connected to an optically isolated constant voltage stimulator under computer control (*69*).

Evoked EMG activity from LG and TA was then recorded during sciatic nerve stimulation. Stimulation and recording were controlled by a laboratory computer system running custom software written in Labview® (Emerson, St. Louis, MO). Ongoing EMG activity in the LG was sampled at 10 kHz; when the rectified and integrated voltage over a 20 msec period fell within a user-defined range, a 0.3 msec duration stimulus pulse was delivered to the nerve via the needle electrodes. Muscle activity was sampled and recorded from 20 msec prior to the stimulus until 100 msec after the stimulus. Stimuli were delivered no more frequently than once every 3 sec to avoid muscle fatigue. A range of stimulus intensities was applied in each experiment to sample evoked muscle activity from sub-threshold to supramaximal. In a typical experiment, approximately 200 stimulus presentations were studied. At the end of each experiment, all electrodes were removed, and the skin was incision closed with sutures.

The recorded compound muscle action potentials (CMAPs) in LG and TA evoked by sciatic nerve stimulation were analyzed off-line. The amplitude of the evoked M waves was measured as the average rectified voltage within a defined time window after the stimulus application. In intact anesthetized animals, this window is 0.5-2 msec. After nerve crush, M waves evoked from sciatic nerve stimulation are, by definition, generated by reinnervated muscle fibers. The latency and duration of these potentials are longer than those found in intact animals (*70*), and thus, the time window used to measure the amplitude of the M waves was adjusted accordingly. Recordings were made from intact

animals, and 2, 4, 6, and 8 wk after nerve crush. At each time point, the amplitude of the largest evoked CMAP was determined and scaled to CMAPs recorded from that animal prior to nerve crush. Means of these scaled responses from animals in which nerves were treated with CPP 168-189 were compared to animals in which nerves were treated with CPP 190-208 at each time studied.

Spinal cord injury stem cell graft **–** Adult female F344 Fischer rats received C4 dorsal column lesion spinal cord injury as previously described (*71*). This injury model transects over 95% of corticospinal axons (*72*). Immediately following injury, rats received transplantation of dissociated neural progenitor cells obtained from the spinal cord (caudalized) or telencephalon (rostralized) of E14 GFP+ F344 rat embryos. Neural progenitor cells were isolated from embryonic tissue by incubation with 0.125% trypsin, gentle mechanical dissociation, and filtering through a 40 µm cell filter as previously described (*71, 73*). A total of 10^6 cells in HBSS were transplanted into the lesion site. Four weeks after SCI and transplantation, rats received cortical injections of 10% biotinylated dextran amine (BDA) across 16 sites into bilateral primary forelimb motor cortices. Animals were sacrificed four weeks later.

Analysis of reticulospinal tract axon regeneration in PNGs **–** For testing expression of G3BP1 B-domain in reticulospinal neurons, AAV5-G3BP1-BFP or AAV5-B domain-BFP was microinjected into the brainstem of female SD (225 g, obtained from Charles River) on day 1 of experimentation. Control rats received AAV5-GFP. Rats received three 1 µl injections at 1 mm rostral-caudal separations into medial-ventral gigantocellular areas of the reticular formation (see Figure 1B). On day 8 the tibial branch of the sciatic nerve of donor SD rats was ligated and cut just distal to its branch point from the sciatic nerve. Seven days later a 10 mm length of degenerated tibial nerve was removed from the donor rat and the distal end was inserted into a C4 hemisection lesion cavity that was prepared by aspiration in a recipient rat. The graft was secured by suturing the perineurium to the dura mater. The distal end of the PNG was left unapposed, lying on top of the adjacent, distal vertebral processes. On day 35 of experimentation (20 days after SCI-PNG) rats were euthanized (see below for details).

For CPP delivery to injured spinal cord axons proximal to PNG, 1 µl of 1 mM 168-189 peptide or 190-208 peptide was microinjected into the spinal cord 1 mm rostral to a fresh C4 hemisection lesion cavity (see Figure 3A). This was estimated to provide a concentration of 28 µM in the tissue. Approximately 20 min later one end of a predegenerated tibial nerve from a donor rat was inserted into the lesion cavity, apposed to the proximal cavity wall and secured by suturing perineurium to the dura mater. The distal end of the PNG was left unapposed, lying on top of the adjacent, distal vertebral processes. On day 18 of experimentation (10 days after SCI-PNG) rats were euthanized (see below for details).

For CPP delivery to regenerating axons within PNGs, 1 µl of 1 mM 190-208 peptide or scrambled peptide was microinjected into the PNG through a fine glass cannula attached to a Hamilton syringe into unapposed distal end of the PNG approximately 30 days after the PNG had been apposed to the rostral wall of the injured C4 spinal cord (see Figure 3E). This was estimated to provide a concentration of 113 µM in the tissue. The cannula tip was inserted horizontally for 2-3 mm into the PNG for peptide injection over a 10-minute period. After withdrawing the cannula, the PNG was moved aside and a 1 mm^3 dorsal quadrant cavity at the C5-6 interface (between entry zones of dorsal root axons) was created by aspiration. The distal end of the PNG was trimmed by 1 mm and inserted into the fresh cavity and secured by suturing perineurium to dura mater. Three weeks after apposing the distal end of the graft rats were euthanized (see below for details).

For all experiments rats received sustained-release Buprenorphine (1 mg/kg, subcutaneously [SC], Zoopharm, Laramie, WY) for analgesia and the antibiotic Cefazolin (160 mg/kg SC 2x daily for 5 days; Sandoz, Princeton, NJ). Two days prior to placement of PNGs rats began a regimen of daily Cyclosporine A injections (10 mg/kg SC; Teva Czech Industries, Sellersville, PA) to prevent graft rejection. At the end of each experiment rats were euthanized with an overdose of Euthasol (390 mg/kg sodium pentobarbital and 50 mg/kg phenytoin, intraperitoneal [IP]), perfused with physiological saline followed

by 4% paraformaldehyde. The spinal cord with attached PNG was removed and transferred to 30% sucrose in 0.1 M phosphate buffer at 4°C before preparing cryostat sections and performing immunohistochemical staining and microscopic analysis.

Optic nerve injury and RGC survival analysis **–** Optic nerve regeneration and RGC survival were investigated in 129s mice using methods that have been previously described (*26, 74-76*). In brief, the optic nerve was exposed and crushed 1-2 mm behind the orbit using jeweler's forceps. In cases involving gene therapy, the gene of interest was packaged into adeno-associated virus (AAV2) at a titer of 10^{12}-10^{13} pfu/ml and injected in a volume of 3 µl intraocularly 2 weeks prior to optic nerve crush (see Figure 1E) to allow time for virally encoded constructs to be expressed within RGCs at adequate levels. Care was taken to avoid injuring the lens, which can profoundly alter levels of axon regeneration (*77*).

After a survival period of 2-3 weeks, mice were euthanized, perfused with saline followed by 4% paraformaldehyde, retinas and optic nerves were dissected and postfixed for 1 h. Optic nerves were equilibrated overnight in 30% sucrose, frozen, sectioned longitudinally at 15 µm on a cryostat, and mounted on coated slides.

Cell culture **–** For primary neuronal cultures, DRGs were harvested in Hibernate-A medium (BrainBits; Cordova, TN) and then dissociated as described (*68*). After centrifugation and washing in DMEM/F12 (Life Technologies), dissociated ganglia were resuspended in DMEM/F12, 1 x N1 supplement (Sigma), 10% fetal bovine serum (Hyclone; Logan, UT), and 10 µM cytosine arabinoside (Sigma). Dissociated DRGs were plated immediately on poly-L-lysine (Sigma) + laminin (Sigma-Millipore, St. Louis, MO) or poly-L-lysine + aggrecan (R&D Systems, Minneapolis, MN) coated surfaces (*20, 68*).

For cortical neuron cultures, E18 rat cortices were dissected in Hibernate E (BrainBits) and dissociated using the *Neural Tissue Dissociation kit* (Miltenyi Biotec, Auburn, CA). For this, minced cortices were incubated in a pre-warmed enzyme mix at 37°C for 15 min; tissues were then triturated and applied to a 40 µm cell strainer. After washing and centrifugation, neurons were seeded on poly-D-

lysine (Sigma) or poly-D-lysine + aggrecan (R&D Systems) coated coverslips. *NbActive-1 medium* (BrainBits) supplemented with 100 U/ml of Penicillin-Streptomycin (Life Technologies), 2 mM L-glutamine (Invitrogen/Thermo-Fisher, Waltham, MA), and 1 X N21 supplement (R&D Systems) was used as culture medium.

The use of human iPSCs was approved by the Institutional Review Board at the University of South Carolina. Human iPSCs from apparently healthy euploid individuals were obtained from Dr. Alberto Costa (Case Western Reserve University; Cleveland, Ohio) (*78*). Cells were maintained in feeder-free culture conditions on Nunc tissue culture-treated 6-well plates (VWR) coated with Matrigel (Corning, Corning, NY). Cells were maintained in mTeSR1 media (StemCell Technologies, Vancouver, Canada) and passaged every 6-7 days using Gentle Cell Dissociation Reagent (StemCell Technologies).

hiPSC-derived cortical neurons were generated using dual SMAD inhibition in a monolayer layer culture, as previously described (*79, 80*). This protocol mainly uses two media formulations – Neuronal Maintenance Media (NMM) and Neuronal Induction Media (NIM). NMM was prepared using 1:1 DMEM/F-12 GlutaMAX:Neurobasal (Gibco/Thermo-Fisher, Waltham, MA), 1x N2 supplement (Gibco), 1x B27 supplement (Gibco), 5 µg/mL insulin (Sigma), 1 mM L-glutamine (Gibco), 500 µM sodium pyruvate (Sigma), 100 µM nonessential amino acids solution (Gibco), 100 µM beta-mercaptoethanol (Gibco), 50 U per mL penicillin-streptomycin (Gibco). NIM was prepared by adding 1 µM Dorsomorphin (Tocris, Minneapolis, MN) and 10 µM SB431542 (Reprocell, Beltsville, MD) to NMM. hiPSCs were plated on matrigel-coated wells of a 6-well plate (day 1). The next day (day 0), when cells were 100% confluent, NIM was added for neuronal induction. Cells were maintained in NIM for 12 days with daily feeding. On day 12, which is characterized by the formation of a neuroepithelial sheet, cells were passaged 1:2 using 1 mg/mL dispase into laminin-coated 6-well dishes. The next day, media was replaced with NMM + 20 ng/mL FGF2, with alternate day feeding. After 4 days of treatment with FGF2, cells were maintained in NMM with alternate day feeding and passaged at a 1:2 split ratio when neuronal rosettes started to

meet. On day 25, cultures were dissociated into single cells using accutase and passaged 1:1 onto laminin-coated 6-well dishes. Following this, the cells were passaged every 2-3 days using accutase at a 1:2 split ratio until approximately day 35. For final plating, cells were passaged using accutase. 10,000 cells were plated in NMM on acid-washed coverslips (15 mm; Carolina Biological, Burlington, NC) pre-coated with 100 µg/mL poly-L-lysine (PLL; Sigma) and 10 µg/mL laminin (Invitrogen/Thermo-Fisher).

For peptide treatments, 10 µM CPPs were added to dissociated DRG cultures, and hiPSCs-derived glutamatergic neuron cultures at 16 h after plating. For embryonic cortical cultures, the peptides were added 10 days after plating. Neurite outgrowth was assessed 48 h after addition of peptides.

Viral expression constructs **–** Generation of the viral constructs has been described previously (*18*). AAV2 and AAV5 preparations were generated in Vigene Biosciences/Charles Rivers Labs (Wilmington, MA) and the viruses were titrated in DRG cultures by incubating with 1.8-2.8 x 10^{10} particles of AAV2/5 overnight.

Generation of Tat-tagged G3BP1 B domain peptides **–** Eight peptides were generated from the rat G3BP1 B domain sequence (amino acids 140-220; UniProt ID # D3ZYS7_RAT) by Peptide 2.0 (Chantilly, VA) and Bachem Americas, Inc. (Torrance, CA). Peptides were synthesized with N-terminal FITC and N- or C-terminal HIV Tat peptide for cell permeability (*81*); the Tat sequence was placed at the least conserved end of the sequence based on P-BLAST of vertebrate G3BP1 sequences available in UniProt database. Peptide sequences were (Tat sequence shown in italics): rodent G3BP1 168-189, DDSGTFYDQTVSNDLEEHLEEP-*YGNKKNNQNNN*; rodent G3BP1 190-208, *YGNKKNNNQNNN*-VVEPEPEPEPEPEPEPVSE; rodent G3BP1 190-208$^{E\rightarrow D}$, *YGNKKNNNQNNN*-VVDPDPDPDPDPDPDPVSD; rodent G3BP1 192-205, *YGNKKNNNQNNN*-EPEPEPEPEPEPEP; human G3BP1 191-209, *YGNKKNNNQNNN*-VAEPEPDPEPEPEQEPVSE; Scramble 190-208, *YGNKKNNNQNNN*-VVEEEEEEEPPPPPPPVSE; and rodent G3BP1 147-166^{S149E}, EEEEEEVEEPEENQQSPEVV-*YGNKKNNQNNN*.

Immunofluorescent staining **–** All procedures were performed at room temperature (RT) unless specified otherwise. Cultured neurons were fixed in 4 % paraformaldehyde (PFA) in phosphate-buffered saline (PBS) and processed as described (*82*). Primary antibodies consisted of: RT97 mouse anti-neurofilament (NF; 1:500; Devel. Studies Hybridoma Bank [DHSB], Iowa City, IA), rabbit anti-βIII Tubulin (1:500; Abcam, Boston, MA), rabbit anti-MAP2 (1:500; Abcam), and SMI312 mouse anti-NF (1:500; Abcam). FITC-conjugated donkey anti-rabbit and Cy3-conjugated donkey anti-mouse (both at 1:200; Jackson ImmunoRes., West Grove, PA) were used as secondary antibodies.

For quantifying axonal content of G3BP1, and TIA1 in sciatic nerves, peripheral nerve grafts, and optic nerves, samples were fixed for 4 h in 4 % PFA and then cryoprotected overnight in 30 % sucrose, PBS at 4°C. 15 µm cryostat sections were processed for immunostaining as previously described (*82*). Primary antibodies consisted of rabbit anti-G3BP1 (1:100; Sigma), goat anti-TIA1 (1:100; SantaCruz Bio., Santa Cruz, CA), and RT97 mouse anti-NF (1:300; DSHB). Secondary antibodies were FITC-conjugated donkey anti-rabbit, FITC-conjugated donkey anti-goat, and Cy3-conjugated donkey anti-mouse (both at 1:200; Jackson ImmunoRes.).

For sciatic nerve regeneration analysis, 15 µm thick cryostat sections of sciatic nerve were processed for immunostaining as previously described (*82*). Primary antibody consisted of rabbit anti-SCG10 (1:200, Abcam). Secondary antibodies were FITC-conjugated donkey anti-rabbit (1:200, Jackson ImmunoRes.).

For reticulospinal tract axon regeneration analysis in PNGs, 15 µm thick cryostat sections were processed for immunostaining. Primary antibody consisted of mouse anti-NF (1:200, DSHB), mouse anti-βIII Tubulin (1:200; Abcam), rabbit anti-SCG10 (1:200; Abcam), rabbit anti-GFP (1:200; Abcam), and rabbit anti-BFP (1:200; Rockland Immuno., Limerick, PA). Secondary antibodies were FITC-conjugated donkey anti-rabbit (1:200; Jackson ImmunoRes.) and Cy3-conjugated donkey anti-mouse (1:200; Jackson ImmunoRes.).

For optic nerve regeneration analysis, 15 µm thick cryostat sections were processed for immunostaining as described previously (*26, 74, 75*). Primary antibody consisted of rabbit anti-BFP (1:200; Rockland) and mouse anti-GAP43 (1:500, Abcam). Secondary antibodies were FITC-conjugated donkey anti-rabbit (1:200; Jackson ImmunoRes.) and Cy3-conjugated donkey anti-mouse (1:200; Jackson ImmunoRes.). For fixed retinas primary antibody consisted of rabbit anti-bIII tubulin (1:100; Abcam), and mouse anti-RBPMS (1:100; Invitrogen). Secondary antibodies were FITC-conjugated donkey anti-rabbit (1:200; Jackson ImmunoRes.) and Cy3-conjugated donkey anti-mouse (1:200; Jackson ImmunoRes.).

All samples were mounted with *Prolong Gold Antifade* (Invitrogen/Thermo-Fisher) and analyzed by epifluorescent or confocal microscopy. Leica DMI6000 epifluorescent microscope with ORCA Flash ER CCD camera (Hamamatsu Photonics, Hamamatusu, Japan), Leica SP8X confocal microscope with HyD detectors, or ImageExpress Micro XLS high content imaging system (Molecular Devices, San Jose, CA) were used for imaging. For quantitation between samples, imaging parameters were matched for exposure, gain, offset and post-processing (*70*). Thus, the time window used to measure the amplitude of the M waves was adjusted to accommodate this change. Recordings were made from intact animals, and 2, 4, 6, and 8 wk after nerve crush. At each time point, the amplitude of the largest evoked M wave (M_{max}) was determined and scaled to M_{max} recorded from that animal prior to nerve crush. Means of these scaled responses recorded from muscles in which motor neurons were treated with the control 168-189 peptide or the 190-208 peptide and were compared at each time studied.

Image analyses and processing **–** For analyses of stress granule protein levels in tissues, z planes of the xyz scans of spinal cord sections were analyzed using *ImageJ. Colocalization Plug-in* was first used to extract G3BP1 signals that overlap with TIA1 and the extracted colocalizing signal was projected as a separate channel. Further, *colocalization Plug-in* was used for the second time, and the G3BP1-TIA1 colocalization channel was overlapped with the axonal marker (NF) in each plane, to extract the 'axon-

only' signal projected as a separate channel (*14*). For calculating axonal G3BP1 granules in PNGs and optic nerves, xyz scans from 2 locations along each nerve section were analyzed using *ImageJ. ImageJ* segmented line tool was used to mark the axons tracking the NF signal and NF overlapping G3BP1 signals were projected as a separate channel. *Image J* particle analyzer was used to quantify the number and size of the granules. The axonal G3BP1 granule number and size were averaged for all image locations in each biological replicate.

For neurite outgrowth, images from 60 h DRG, or hiPSCs, and 12 days cortical cultures images were analyzed for neurite length and branching using *WIS-Neuromath* (*83*) with NF, Tubulin βIII, SMI312 immunostained cultures. For reticulospinal axon branching in analyses, high resolution confocal microscopy of the 0 mm PNG sections was performed and further analyzed using Neurolucida 360 and Neurolucida Explorer software (MBF Bioscience, VT). Branching complexity was assessed using the default software parameters.

For optic nerve regeneration analysis, confocal microscopy of anti-GFP/BFP and -GAP43 immunostained optic nerve sections were performed and GAP43-positive regenerating axons were counted manually at 0, 0.5, 1, 1.5 and 2.0 mm from the injury site. 4-5 sections/animal were counted and the number of axons in the entire nerve was estimated using as described (*26*).

For RGC survival analysis, fixed retinas were immunostained for Tubulin βIII and RBPMS and were divided into four quadrants with radial relieving cuts, mounted on prepared slides, and RGC survival was evaluated by counting the number of RBPMS positive stained cells/mm^2 in 8 pre-specified areas of retina (2 areas in each quadrant at 1.0 and 2.0 mm from the center).

To assess regeneration *in vivo*, tile scans of SCG10-stained nerve sections were post-processed by *ImageJ Straighten Plug-in* (http://imagej.nih.gov/ij/). NF positive axon profiles (>30 µm long) were then counted in 30 µm bins at 0.25 mm intervals proceeding distally from the crush site. Crush site was identified by SCG10 staining and DIC imaging. Axon profiles present in the proximal crush site was

treated as the baseline, and values from the distal bins were normalized to this to calculate the percentage of regenerating axon profiles.

Statistical analyses **–** *Prism* (GraphPad, La Jolla, CA) and *Excel* (Microsoft, Redmond, WA) software packages were used for statistical analyses. One-way ANOVA or Two-way ANOVA was used to compare means of > 2 independent groups and Student's *t*-test was used to compare between 2 groups. *p* values of ≤ 0.05 were considered as statistically significant. Z scores were calculated using the formula $\{\frac{x-\mu}{\sigma}\}$, where x = sample mean, μ = population mean, and σ = population standard deviation.

LIST OF EXTENDED DATA

Extended Data Figure 1: *Expression of G3BP1 acidic domain increases RGC survival after optic nerve injury.*

Extended Data Figure 2: *G3BP1 B domain expression reduces G3BP1 granules in reticulospinal and optic nerve axons.*

Extended Data Figure 3: *G3BP1 190-208 cell permeable peptide promotes axon growth.*

Extended Data Figure 4: *Rat and human G3BP1 cell permeable peptides promote axon growth from human iPSC-derived glutamatergic neurons.*

Extended Data Figure 5: *G3BP1 cell permeable peptide increases axon branching on growth-inhibitory substrate.*

REFERENCES

1. A. Hoke, Mechanisms of Disease: what factors limit the success of peripheral nerve regeneration in humans? *Nat Clin Pract Neurol* **2**, 448-454 (2006).

2. J. W. Fawcett, The Struggle to Make CNS Axons Regenerate: Why Has It Been so Difficult? *Neurochem Res* **45**, 144-158 (2020).

3. Y. Ohtake *et al.*, The effect of systemic PTEN antagonist peptides on axon growth and functional recovery after spinal cord injury. *Biomaterials* **35**, 4610-4626 (2014).

4. N. Abe, S. H. Borson, M. J. Gambello, F. Wang, V. Cavalli, mTOR activation increases axonal growth capacity of injured peripheral nerves. *J Biol Chem* **285**, 28034-28043 (2010).

5. K. J. Christie, C. A. Webber, J. A. Martinez, B. Singh, D. W. Zochodne, PTEN inhibition to facilitate intrinsic regenerative outgrowth of adult peripheral axons. *J Neurosci* **30**, 9306-9315 (2010).

6. C. A. Danilov, O. Steward, Conditional genetic deletion of PTEN after a spinal cord injury enhances regenerative growth of CST axons and motor function recovery in mice. *Exp Neurol* **266**, 147-160 (2015).

7. K. Liu *et al.*, PTEN deletion enhances the regenerative ability of adult corticospinal neurons. *Nat Neurosci* **13**, 1075-1081 (2010).

8. K. K. Park, K. Liu, Y. Hu, J. L. Kanter, Z. He, PTEN/mTOR and axon regeneration. *Exp Neurol* **223**, 45-50 (2010).

9. K. K. Park *et al.*, Promoting axon regeneration in the adult CNS by modulation of the PTEN/mTOR pathway. *Science* **322**, 963-966 (2008).

10. T. P. Smith, P. K. Sahoo, A. N. Kar, J. L. Twiss, Intra-axonal mechanisms driving axon regeneration. *Brain Res* **1740**, 146864 (2020).

11. H. H. Wong *et al.*, RNA Docking and Local Translation Regulate Site-Specific Axon Remodeling In Vivo. *Neuron* **95**, 852-868 e858 (2017).

12. T. Shigeoka *et al.*, Dynamic Axonal Translation in Developing and Mature Visual Circuits. *Cell* **166**, 181-192 (2016).

13. H. Jung, B. C. Yoon, C. E. Holt, Axonal mRNA localization and local protein synthesis in nervous system assembly, maintenance and repair. *Nat Rev Neurosci* **13**, 308-324 (2012).

14. A. L. Kalinski *et al.*, mRNAs and Protein Synthetic Machinery Localize into Regenerating Spinal Cord Axons When They Are Provided a Substrate That Supports Growth. *J Neurosci* **35**, 10357-10370 (2015).

15. B. A. Walker *et al.*, Reprogramming axonal behavior by axon-specific viral transduction. *Gene Ther* **19**, 947-955 (2012).

16. R. Sachdeva, K. Farrell, M. K. McMullen, J. L. Twiss, J. D. Houle, Dynamic Changes in Local Protein Synthetic Machinery in Regenerating Central Nervous System Axons after Spinal Cord Injury. *Neural Plast* **2016**, 4087254 (2016).

17. D. E. Willis *et al.*, Axonal Localization of transgene mRNA in mature PNS and CNS neurons. *J Neurosci* **31**, 14481-14487 (2011).

18. P. K. Sahoo *et al.*, Axonal G3BP1 stress granule protein limits axonal mRNA translation and nerve regeneration. *Nat Commun* **9**, 3358 (2018).

19. P. Anderson, N. Kedersha, RNA granules: post-transcriptional and epigenetic modulators of gene expression. *Nat Rev Mol Cell Biol* **10**, 430-436 (2009).

20. P. Sahoo *et al.*, A translational switch drives axonal stress granule disassembly through Casein Kinase 2α. *Curr Biol* **30**, 4882-4895.E4886 (2020).

21. P. Lu *et al.*, Long-distance growth and connectivity of neural stem cells after severe spinal cord injury. *Cell* **150**, 1264-1273 (2012).

22. J. F. Bonner *et al.*, Grafted Neural Progenitors Integrate and Restore Synaptic Connectivity across the Injured Spinal Cord. *J Neurosci* **31**, 4675-4686 (2011).

23. N. M. Tran *et al.*, Single-Cell Profiles of Retinal Ganglion Cells Differing in Resilience to Injury Reveal Neuroprotective Genes. *Neuron* **104**, 1039-1055 e1012 (2019).

24. E. R. Bray *et al.*, Thrombospondin-1 Mediates Axon Regeneration in Retinal Ganglion Cells. *Neuron* **103**, 642-657 e647 (2019).

25. Y. Hu *et al.*, Differential effects of unfolded protein response pathways on axon injury-induced death of retinal ganglion cells. *Neuron* **73**, 445-452 (2012).

26. S. Leon, Y. Yin, J. Nguyen, N. Irwin, L. I. Benowitz, Lens injury stimulates axon regeneration in the mature rat optic nerve. *J Neurosci* **20**, 4615-4626 (2000).

27. D. S. Smith, P. Skene, A transcription-dependent switch controls competence of adult neurons for distinct modes of axon growth. *J Neurosci* **17**, 646-658. (1997).

28. J. Q. Zheng *et al.*, A functional role for intra-axonal protein synthesis during axonal regeneration from adult sensory neurons. *J Neurosci* **21**, 9291-9303 (2001).

29. D. Vuppalanchi *et al.*, Conserved 3'-untranslated region sequences direct subcellular localization of chaperone protein mRNAs in neurons. *J Biol Chem* **285**, 18025-18038 (2010).

30. S. Stern *et al.*, RhoA drives actin compaction to restrict axon regeneration and astrocyte reactivity after CNS injury. *Neuron* **109**, 3436-3455 e3439 (2021).

31. B. A. Walker, S. J. Ji, S. R. Jaffrey, Intra-axonal translation of RhoA promotes axon growth inhibition by CSPG. *J Neurosci* **32**, 14442-14447 (2012).

32. J. Ng *et al.*, Rac GTPases control axon growth, guidance and branching. *Nature* **416**, 442-447 (2002).

33. S. Tivodar *et al.*, Rac-GTPases Regulate Microtubule Stability and Axon Growth of Cortical GABAergic Interneurons. *Cereb Cortex* **25**, 2370-2382 (2015).

34. S. J. Lee *et al.*, Selective axonal translation of the mRNA isoform encoding prenylated Cdc42 supports axon growth. *J Cell Sci* **134**, (2021).

35. M. L. Pearn *et al.*, Inhibition of RhoA reduces propofol-mediated growth cone collapse, axonal transport impairment, loss of synaptic connectivity, and behavioural deficits. *Br J Anaesth* **120**, 745-760 (2018).

36. R. E. Gross, Q. Mei, C. A. Gutekunst, E. Torre, The pivotal role of RhoA GTPase in the molecular signaling of axon growth inhibition after CNS injury and targeted therapeutic strategies. *Cell Transplant* **16**, 245-262 (2007).

37. M. A. Kopp *et al.*, Small-molecule-induced Rho-inhibition: NSAIDs after spinal cord injury. *Cell Tissue Res* **349**, 119-132 (2012).

38. M. G. Andrusiak *et al.*, Inhibition of Axon Regeneration by Liquid-like TIAR-2 Granules. *Neuron* **104**, 290-304 (2019).

39. S. Neumann, C. J. Woolf, Regeneration of dorsal column fibers into and beyond lesion site following adult spinal cord injury. *Neuron* **23**, 83-91 (1999).

40. L. I. Benowitz, L. Xie, Y. Yin, Inflammatory Mediators of Axon Regeneration in the Central and Peripheral Nervous Systems. *Int J Mol Sci* **24**, (2023).

41. J. Yang, Y. Yin, PTEN in Chromatin Remodeling. *Cold Spring Harb Perspect Med* **10**, (2020).

42. J. O. Lipton, M. Sahin, The neurology of mTOR. *Neuron* **84**, 275-291 (2014).

43. M. Terenzio *et al.*, Locally translated mTOR controls axonal local translation in nerve injury. *Science* **359**, 1416-1421 (2018).

44. M. J. Kye *et al.*, SMN regulates axonal local translation via miR-183/mTOR pathway. *Hum Mol Genet* **23**, 6318-6331 (2014).

45. A. Poulopoulos *et al.*, Subcellular transcriptomes and proteomes of developing axon projections in the cerebral cortex. *Nature* **565**, 356-360 (2019).

46. P. Yang *et al.*, G3BP1 Is a Tunable Switch that Triggers Phase Separation to Assemble Stress Granules. *Cell* **181**, 325-345 e328 (2020).

47. C. UniProt, UniProt: the Universal Protein Knowledgebase in 2023. *Nucleic Acids Res* **51**, D523-D531 (2023).

48. J. Guillen-Boixet *et al.*, RNA-Induced Conformational Switching and Clustering of G3BP Drive Stress Granule Assembly by Condensation. *Cell* **181**, 346-361 e317 (2020).

49. K. Stillger, I. Neundorf, Cell-permeable peptide-based delivery vehicles useful for subcellular targeting and beyond. *Cell Signal* **109**, 110796 (2023).

50. N. Lev *et al.*, A DJ-1 Based Peptide Attenuates Dopaminergic Degeneration in Mice Models of Parkinson's Disease via Enhancing Nrf2. *PLoS One* **10**, e0127549 (2015).

51. C. Marelli, F. Maschat, The P42 peptide and Peptide-based therapies for Huntington's disease. *Orphanet J Rare Dis* **11**, 24 (2016).

52. T. Altman *et al.*, Axonal TDP-43 condensates drive neuromuscular junction disruption through inhibition of local synthesis of nuclear encoded mitochondrial proteins. *Nat Commun* **12**, 6914 (2021).

53. S. Elmsaouri, S. Markmiller, G. W. Yeo, APEX Proximity Labeling of Stress Granule Proteins. *Methods Mol Biol* **2428**, 381-399 (2022).

54. S. Hu *et al.*, Time-resolved proteomic profiling reveals compositional and functional transitions across the stress granule life cycle. *Nat Commun* **14**, 7782 (2023).

55. H. Marmor-Kollet *et al.*, Spatiotemporal Proteomic Analysis of Stress Granule Disassembly Using APEX Reveals Regulation by SUMOylation and Links to ALS Pathogenesis. *Mol Cell* **80**, 876-891.e876 (2020).

56. Y. C. Liao *et al.*, RNA Granules Hitchhike on Lysosomes for Long-Distance Transport, Using Annexin A11 as a Molecular Tether. *Cell* **179**, 147-164 e120 (2019).

57. A. Lamiable *et al.*, PEP-FOLD3: faster de novo structure prediction for linear peptides in solution and in complex. *Nucleic Acids Res* **44**, W449-454 (2016).

58. Y. Shen, J. Maupetit, P. Derreumaux, P. Tuffery, Improved PEP-FOLD Approach for Peptide and Miniprotein Structure Prediction. *J Chem Theory Comput* **10**, 4745-4758 (2014).

59. P. Thevenet *et al.*, PEP-FOLD: an updated de novo structure prediction server for both linear and disulfide bonded cyclic peptides. *Nucleic Acids Res* **40**, W288-293 (2012).

60. Y. Fujita, T. Yamashita, Axon growth inhibition by RhoA/ROCK in the central nervous system. *Front Neurosci* **8**, 338 (2014).

61. K. Y. Wu *et al.*, Local translation of RhoA regulates growth cone collapse. *Nature* **436**, 1020-1024 (2005).

62. S. P. Somasekharan *et al.*, G3BP1-linked mRNA partitioning supports selective protein synthesis in response to oxidative stress. *Nucleic Acids Res* **48**, 6855-6873 (2020).

63. E. W. Dent, K. Kalil, Axon branching requires interactions between dynamic microtubules and actin filaments. *J Neurosci* **21**, 9757-9769 (2001).

64. D. M. Snow, P. B. Atkinson, T. D. Hassinger, P. C. Letourneau, S. B. Kater, Chondroitin sulfate proteoglycan elevates cytoplasmic calcium in DRG neurons. *Dev Biol* **166**, 87-100 (1994).

65. A. L. Kalinski *et al.*, Deacetylation of Miro1 by HDAC6 blocks mitochondrial transport and mediates axon growth inhibition. *J Cell Biol* **218**, 1871-1890 (2019).

66. N. P. Tsai, L. N. Wei, RhoA/ROCK1 signaling regulates stress granule formation and apoptosis. *Cell Signal* **22**, 668-675 (2010).

67. J. Gal *et al.*, The Acetylation of Lysine-376 of G3BP1 Regulates RNA Binding and Stress Granule Dynamics. *Mol Cell Biol* **39**, e00052-00019 (2019).

68. J. L. Twiss, D. S. Smith, B. Chang, E. M. Shooter, Translational control of ribosomal protein L4 mRNA is required for rapid neurite regeneration. *Neurobiol Dis* **7**, 416-428 (2000).

69. P. J. Ward, A. W. English, Optical Stimulation and Electrophysiological Analysis of Regenerating Peripheral Axons. *Bio Protoc* **9**, (2019).

70. A. W. English, Y. Chen, J. S. Carp, J. R. Wolpaw, X. Y. Chen, Recovery of electromyographic activity after transection and surgical repair of the rat sciatic nerve. *J Neurophysiol* **97**, 1127-1134 (2007).

71. J. N. Dulin *et al.*, Injured adult motor and sensory axons regenerate into appropriate organotypic domains of neural progenitor grafts. *Nat Commun* **9**, 84 (2018).

72. N. Weidner, A. Ner, N. Salimi, M. H. Tuszynski, Spontaneous corticospinal axonal plasticity and functional recovery after adult central nervous system injury. *Proc Natl Acad Sci U S A* **98**, 3513-3518 (2001).

73. P. Lu *et al.*, Motor axonal regeneration after partial and complete spinal cord transection. *J Neurosci* **32**, 8208-8218 (2012).

74. Y. Yin *et al.*, Oncomodulin is a macrophage-derived signal for axon regeneration in retinal ganglion cells. *Nat Neurosci* **9**, 843-852 (2006).

75. S. de Lima *et al.*, Full-length axon regeneration in the adult mouse optic nerve and partial recovery of simple visual behaviors. *Proc Natl Acad Sci U S A* **109**, 9149-9154 (2012).

76. L. Xie *et al.*, Monocyte-derived SDF1 supports optic nerve regeneration and alters retinal ganglion cells' response to Pten deletion. *Proc Natl Acad Sci U S A* **119**, e2113751119 (2022).

77. Q. Feng, K. A. Wong, L. I. Benowitz, Full-length optic nerve regeneration in the absence of genetic manipulations. *JCI Insight* **8**, (2023).

78. M. L. Y, B. L. Zampieri, J. J. Scott-McKean, M. W. Johnson, A. C. S. Costa, Generation of Integration-Free Induced Pluripotent Stem Cells from Urine-Derived Cells Isolated from Individuals with Down Syndrome. *Stem Cells Transl Med* **6**, 1465-1476 (2017).

79. Y. Shi, P. Kirwan, F. J. Livesey, Directed differentiation of human pluripotent stem cells to cerebral cortex neurons and neural networks. *Nat Protoc* **7**, 1836-1846 (2012).

80. V. Volpato *et al.*, Reproducibility of Molecular Phenotypes after Long-Term Differentiation to Human iPSC-Derived Neurons: A Multi-Site Omics Study. *Stem Cell Reports* **11**, 897-911 (2018).

81. M. Aarts *et al.*, Treatment of ischemic brain damage by perturbing NMDA receptor- PSD-95 protein interactions. *Science* **298**, 846-850 (2002).

82. T. T. Merianda, C. Gomes, S. Yoo, D. Vuppalanchi, J. L. Twiss, Axonal localization of neuritin/CPG15 mRNA in neuronal populations through distinct 5' and 3' UTR elements. *J Neurosci* **33**, 13735-13742 (2013).

83. I. Rishal *et al.*, WIS-NeuroMath enables versatile high throughput analyses of neuronal processes. *Dev Neurobiol* **73**, 247-256 (2013).

Competing Interests: PK Sahoo and JL Twiss hold a US patent on use of the G3BP1 cell permeable peptide for axon regeneration and neurodegeneration.

Acknowledgements: The authors thank members of the K. Welshhans, F. Poulain and D.S. Smith laboratories at the University of South Carolina for constructive discussion. JL Twiss is the incumbent SmartState Chair in Childhood Neurotherapeutics at the University of South Carolina.

Funding: This work was supported by grants from the National Institutes of Neurological Disorders and Stroke of the NIH (R01-NS0117821 to JLT, PW, AE, and JDH), the Dr. Miriam and Sheldon G. Adelson Medical Research Foundation (to JLT, MT, and AB), the Craig H. Neilsen Foundation (733151 to JLT and JND), the South Carolina Spinal Cord Injury Research Fund (to PKS and JLT), the Merkin Peripheral Neuropathy and Nerve Regeneration Center (to PKS), and the University of South Carolina Vice President for Research Office (JLT).

Author contributions:

Conceptualization – PKS, JDH, JLT
Methodology – PKS, NH, PW, MA, JDH
Investigation – PKS, NJ, PW, MA, JDH
Visualization – PKS, JLT
Funding acquisition – PKS, JND, MT, KW, LB, AE, JDH, JLT
Project administration – JLT
Supervision – JND, MT, KW, LB, AE, JDH, JLT
Writing, original draft – PKS, JND, JDH, PW, JLT
Writing, review & editing – NH, PW, MA, JND, MT, KW, LB, AE, JDH

Data and materials availability: The data that support the findings of this study are available from the corresponding author upon reasonable request. PKS and JLT hold a US patent on use of the G3BP1 cell permeable peptide for axon regeneration. So, request for this reagent will be available by materials transfer agreements (MTAs) with the University of South Carolina.

FIGURE LEGENDS

Figure 1: ***Expression of G3BP1 acidic domain in CNS neurons facilitates axon regeneration.***

A, Representative exposure-matched confocal images of corticospinal axons in spinal cord labeled with biotinylated dextran amine (BDA) following C4 level contusion injury and subsequent grafting with rostralized or caudalized stem cell graft (*21*). Upper row shows XY optical plane through CST axon regenerating into graft; lower row shows signals for stress granule proteins G3BP1 and TIA1 that overlap with BDA across Z sections as XYZ projection in a separate channel ('axonal G3BP1 + TIA1') [scale bar = 10 µm]. There are stress granules present in the few axons regenerating into rostralized grafts, and these are absent in the more numerous axons regenerating into caudalized grafts.

B, Schematic of experimental paradigm and timeline for spinal cord injury model used in C-D, with regeneration of reticulospinal neurons in the permissive environment of a peripheral nerve graft (PNG).

C, Exposure-matched epifluorescence images for NF- + βIII Tubulin-immunostained PNGs from animals transduced with AAV5-GFP, -G3BP1-BFP, or -G3BP1 B domain-BFP shown at indicated distances from grafting site at proximal side of transected spinal cord [scale bar = 500 µm]. For G3BP1 granule size and density after CPP treatment see Extended Data Figure 2A-C.

D, Quantitation of regenerating reticulospinal axon profile numbers in PNGs from panel C at indicated distances away from grafting site in spinal cord shown as mean ± standard error of the mean (SEM; N = 5 animals; *$p \leq 0.05$ vs. GFP- and & $p \leq 0.05$ vs. G3BP1-BFP by two-way ANOVA with Tukey HSD post-hoc).

E, Schematic of experimental paradigm for AAV transduction of retinal ganglion cells (RGC) and optic nerve crush injury used in F-G.

F, Confocal montage images of optic nerves for AAV2-GFP, -G3BP1-BFP, G3BP1 B-domain-BFP transduced animals at 14 days post injury. Regenerating axons are detected by anti-GAP43 (red) and

GFP, G3BP1-BFP and G3BP1 B-domain-BFP signals by anti-BFP/GFP antibodies (green) [scale bar = 250 µm]. For G3BP1 granule size and density after CPP treatment see Extended Data Figure 2D-F.

G, Quantitation of GAP43 signals from F for regenerating RGC axon profiles is shown as mean ± SEM (N ≥ 5 animals; **p ≤ 0.01 and ****p ≤ 0.0001 vs. GFP- and && p ≤ 0.01 and &&&& p ≤ 0.001 vs. G3BP1-BFP-transduced animals by two-way ANOVA with Tukey HSD post-hoc). For RGC survival data see Extended Data Figure 1.

Figure 2: ***G3BP1 190-208 peptide promotes PNS and CNS axon growth.***

A, Schematic of rat G3BP1 protein with defined domains shown on the top. Sequence of acidic domain (B domain) of G3BP1 shown below with sequence of amino acids 147-166, 168-189 and 190-208 used for cell permeable peptides (CPP) with residue variations shown in fuscia. Variants of these CPPs tested in panels F-G and Extended Data Figures 3-4 are indicated.

B, Timeline for sciatic nerve injury followed by intra-nerve G3BP1 CPP treatments used for panels C-E and Extended Data Figure 3A.

C-D, Exposure-matched epifluorescence images for anti-SCG10 immunostained sciatic nerves 7 days post-crush that were treated with indicated CPPs or PBS are shown in **C**. Dotted line shows the injury site. Quantitation of SCG10+ axon profiles at indicated distances past the injury site from C is shown in **D** as mean ± SEM (N ≥ 6 animals; * p ≤ 0.05 by two-way ANOVA vs. 168-189 with Tukey HSD post-hoc) [scale bar = 500 µm].

E, Compound muscle action potentials (CMAP) are shown for gastrocnemius muscle of animals treated with G3BP1 CPPs after sciatic nerve crush injury as in B are shown as average % intact M responses ± SEM for indicated times (N ≥ 4 animals; *p ≤ 0.05 by Student's t-test for indicated data pairs). For CMAP data on tibialis anterior muscle see Extended Data Figure 3A.

F, Quantitation of total axon growth of cultured adult rat sensory (DRG) neurons treated with G3BP1 CPP and variants is shown as mean ± SEM (left Y-axis) and Z score relative to population mean (right Y-

axis; N ≥ 352 neurons across three biological replicates for each condition; * p ≤ 0.05 and **** p ≤ 0.0001 vs. 168-189 CPP by one-way ANOVA with Dunnett post-hoc). Representative images and data on longest axon per neuron and branch density are shown in Extended Data Figure 3.

G, Quantitation of total neurite length for human iPSC (hiPSC)-derived glutamatergic neurons treated with indicated G3BP1 CPPs and variants shown as mean ± SEM (left Y-axis) and Z score vs. population mean (right Y-axis; N ≥ 1165 neurons across three biological replicates for each condition; **** p ≤ 0.0001 vs. 168-189 CPP by one-way ANOVA with Tukey HSD post-hoc). Representative images plus longest neurite length and neurite branching data are shown in Extended Data Figure 4.

Figure 3: ***G3BP1 190-208 cell permeable peptide promotes in vivo CNS axon regeneration.***

A, Schematic of experimental paradigm for spinal cord injury plus PNG and CPP treatment into spinal cord just rostral to injury site used in B-D.

B, Quantitation of regenerating reticulospinal axon profiles into PNGs from panel B at indicated distances from spinal cord shown as mean ± SEM (N = 5 animals; *p ≤ 0.05 by Student's t-test for indicated data pairs).

C, Neurolucida tracing images for NF- + -βIII tubulin-immunostained reticulospinal axons in proximal PNG shown. Primary branches are pseudo-colored as cyan and secondary/tertiary branches are pseudo-colored from violet-to-magenta. Note increased violet to magenta neurites in the G3BP1 190-208 CPP- vs. 168-189 CPP-treated animals indicating increased branching [scale bar = 250 µm in large images and 25 µm in insets].

D, Quantitation of axonal branching from Neurolucida tracing from C shown as mean ± SEM (N = 5 animals; *p ≤ 0.05 by Student's t-test).

E, Schematic of experimental paradigm for spinal cord injury plus PNG and CPP treatment into the PNG used in F-G is shown.

F, Representative fluorescent images show anti-SCG10 immunosignals for regenerating reticulospinal axons in PNGs. Yellow dotted line shows the junction between PNG and spinal cord, with many more axons penetrating the spinal cord in G3BP1 190-208 CPP- than scrambled 190-208 (Scr 190-208 [E_7P_7])-treated animals [scale bar = 50 µm].

G, Quantitation of distal spinal cord reticulospinal axons from F shown as mean ± SEM (N = 6 animals; ***p ≤ 0.001 by Student's t-test).

<u>Figure 4</u>: ***G3BP1 acidic domain inhibits axonal G3BP1 granule assembly to enable CNS axon regeneration.***

A-B, Axon and dendrite length and branching for G3BP1 190-208 vs. 168-189 CPP-treated E18 rat cortical neurons cultured on growth-permissive (**A**; PDL) vs. growth-inhibitory (**B**; PDL + aggrecan) substrates is shown as mean ± SEM. Note that axon and dendrite branching are significantly increased on the growth inhibitory substrates with 190-208 CPP exposure (N ≥ 1042 neurons across 3 culture preparations for each condition; **** p ≤ 0.0001 by students T-test). Axon morphologies for adult DRG cultured on aggrecan plus G3BP1 190-208 vs. 168-189 CPP shown in Extended Data Figure 5C-D.

C, Representative epifluorescence images of SMI312 immunostained E18 rat cortical neurons cultured on aggrecan and treated with G3BP1 190-208 CPP vs. scrambled 190-208 CPP ± 10 µM RhoA inhibitor shown [scale bar = 50 µm].

D, Quantitation of axon length and branching density for E18 cortical neurons as in C shown as mean ± SEM (N ≥ 259 neurons across three repetitions for each condition; ****p ≤ 0.0001 by one-way ANOVA with Tukey HSD post-hoc). Average length axons extend beyond soma shown in Extended Data Figure 5E.

Figure 1

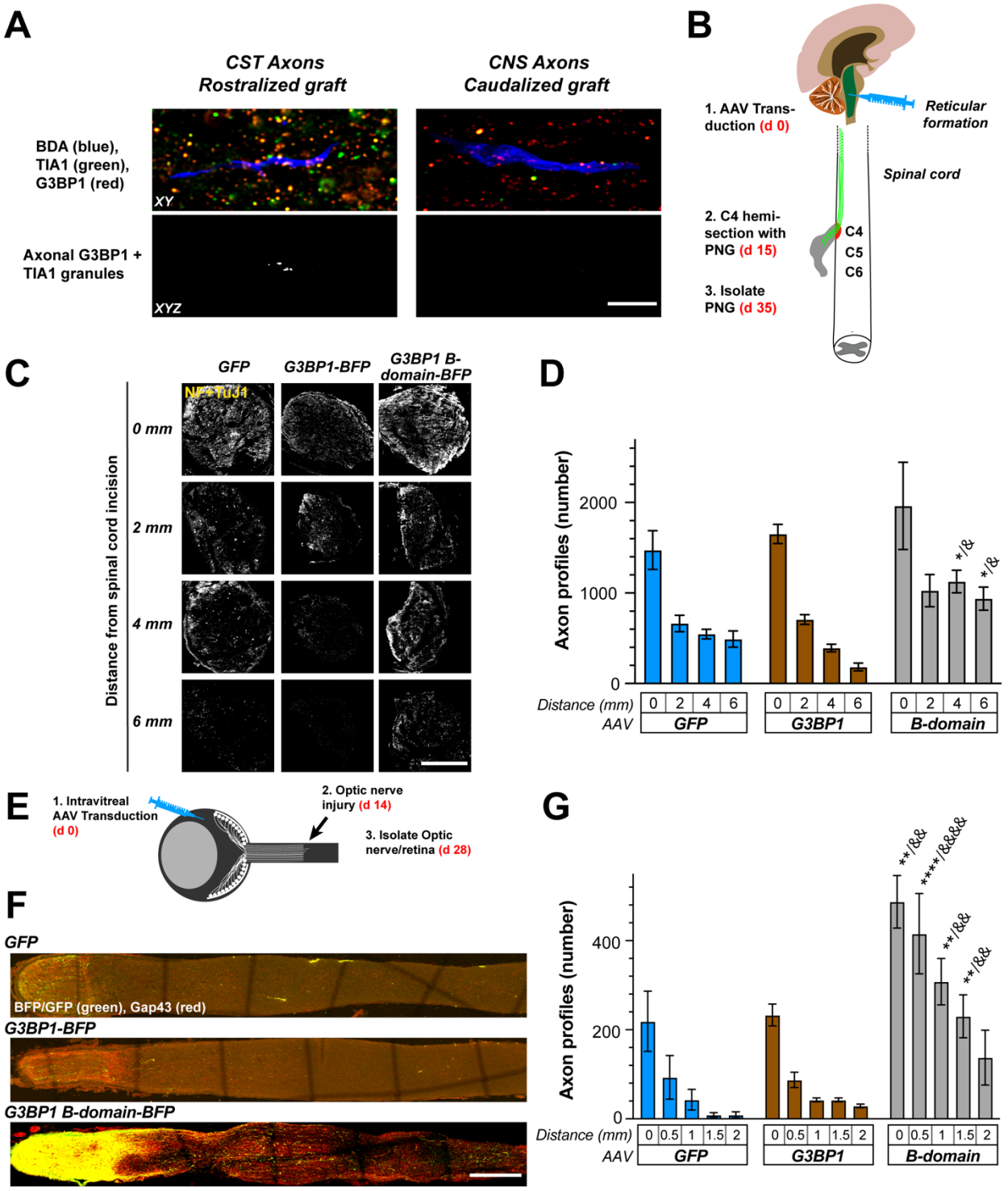
A
CST Axons
Rostralized graft
CNS Axons
Caudalized graft
BDA (blue), TIA1 (green), G3BP1 (red)
XY
Axonal G3BP1 + TIA1 granules
XYZ
B
1. AAV Trans-duction (d 0)
Reticular formation
Spinal cord
2. C4 hemi-section with PNG (d 15)
C4
C5
C6
3. Isolate PNG (d 35)
C
GFP
G3BP1-BFP
G3BP1 B-domain-BFP
NF+TuJ1
Distance from spinal cord incision
0 mm
2 mm
4 mm
6 mm
D
Axon profiles (number)
2000
1000
0
*/&
*/&
Distance (mm)
AAV
0 2 4 6
GFP
G3BP1
B-domain
E
1. Intravitreal AAV Transduction (d 0)
2. Optic nerve injury (d 14)
3. Isolate Optic nerve/retina (d 28)
F
GFP
BFP/GFP (green), Gap43 (red)
G3BP1-BFP
G3BP1 B-domain-BFP
G
Axon profiles (number)
400
200
0
**/&&
****/&&&&
**/&&
**/&&
Distance (mm)
AAV
0 0.5 1 1.5 2
GFP
G3BP1
B-domain

Figure 2

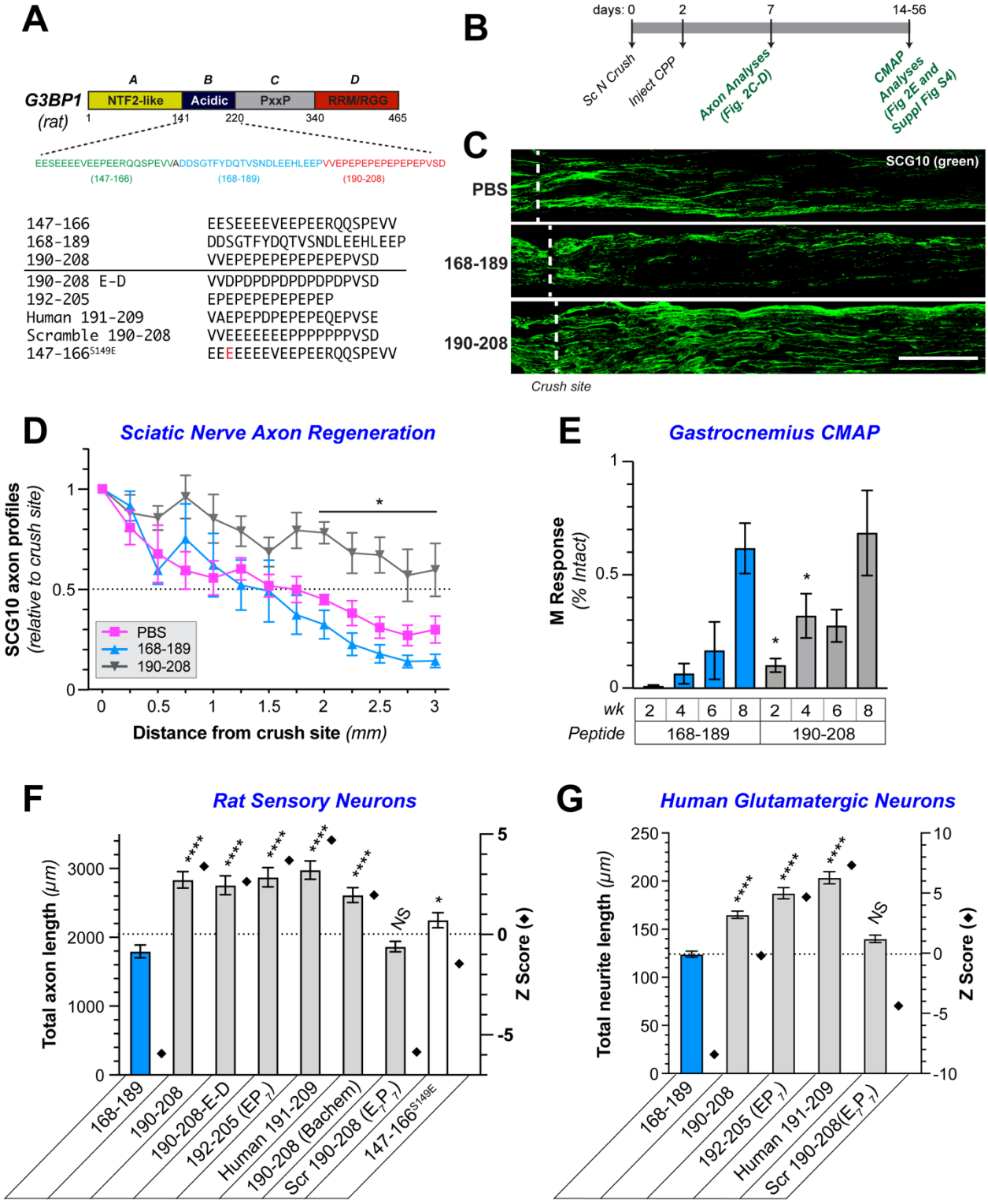
A
G3BP1 (rat)
A B C D
NTF2-like
Acidic
PxxP
RRM/RGG
1 141 220 340 465
EESEEEEVEEPEERQQSPEVVADDSGTFYDQTVSNDLEEHLEEPVVEPEPEPEPEPEPEPVSD
(147-166)
(168-189)
(190-208)
147-166 EESEEEEVEEPEERQQSPEVV
168-189 DDSGTFYDQTVSNDLEEHLEEP
190-208 VVEPEPEPEPEPEPEPVSD
190-208 E-D VVDPDPDPDPDPDPDPVSD
192-205 EPEPEPEPEPEPEP
Human 191-209 VAEPEPDPEPEPEQEPVSE
Scramble 190-208 VVEEEEEEEPPPPPPPVSD
147-166S149E EEEEEEEVEEPEERQQSPEVV
B
days: 0 2 7 14-56
Sc N Crush
Inject CPP
Axon Analyses (Fig. 2C-D)
CMAP Analyses (Fig 2E and Suppl Fig S4)
C
SCG10 (green)
PBS
168-189
190-208
Crush site
D
Sciatic Nerve Axon Regeneration
SCG10 axon profiles (relative to crush site)
Distance from crush site (mm)
PBS
168-189
190-208
E
Gastrocnemius CMAP
M Response (% Intact)
wk 2 4 6 8 2 4 6 8
Peptide 168-189 190-208
F
Rat Sensory Neurons
Total axon length (μm)
Z Score (◆)
168-189
190-208
190-208-E-D
192-205 (EP 7)
Human 191-209
190-208 (Bachem)
Scr 190-208 (E7P 7)
147-166S149E
G
Human Glutamatergic Neurons
Total neurite length (μm)
Z Score (◆)
168-189
190-208
192-205 (EP 7)
Human 191-209
Scr 190-208(E7P 7)

Figure 3

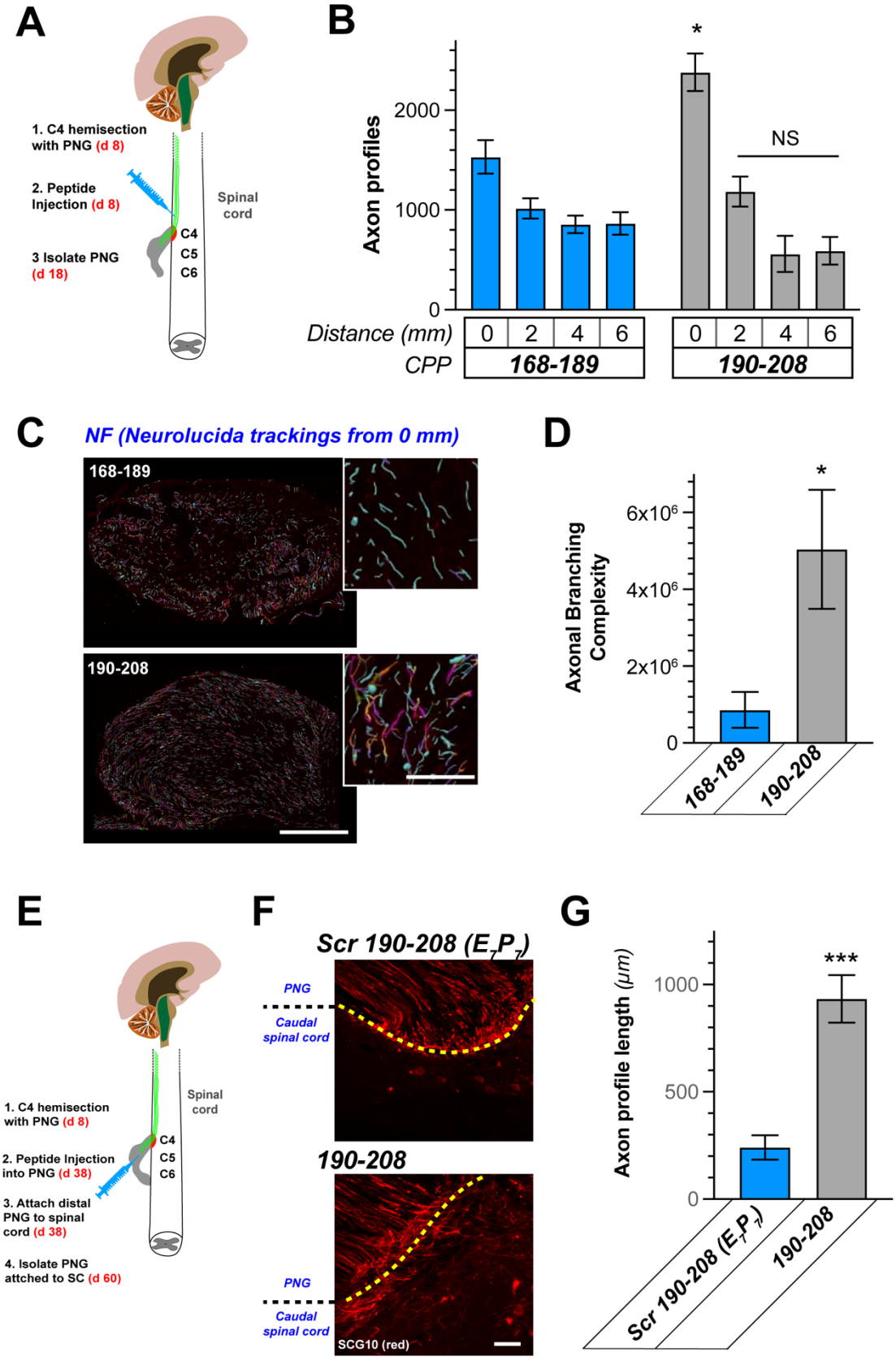
A
1. C4 hemisection with PNG (d 8)
2. Peptide Injection (d 8)
3 Isolate PNG (d 18)
Spinal cord
C4
C5
C6
B
Axon profiles
2000
1000
0
*
NS
Distance (mm)
0 2 4 6
0 2 4 6
CPP
168-189
190-208
C
NF (Neurolucida trackings from 0 mm)
168-189
190-208
D
Axonal Branching Complexity
6x10⁶
4x10⁶
2x10⁶
0
*
168-189
190-208
E
1. C4 hemisection with PNG (d 8)
2. Peptide Injection into PNG (d 38)
3. Attach distal PNG to spinal cord (d 38)
4. Isolate PNG attched to SC (d 60)
Spinal cord
C4
C5
C6
F
Scr 190-208 (E7P7)
PNG
Caudal spinal cord
190-208
PNG
Caudal spinal cord
SCG10 (red)
G
Axon profile length (μm)
1000
500
0
***
Scr 190-208 (E7P7)
190-208

Figure 4

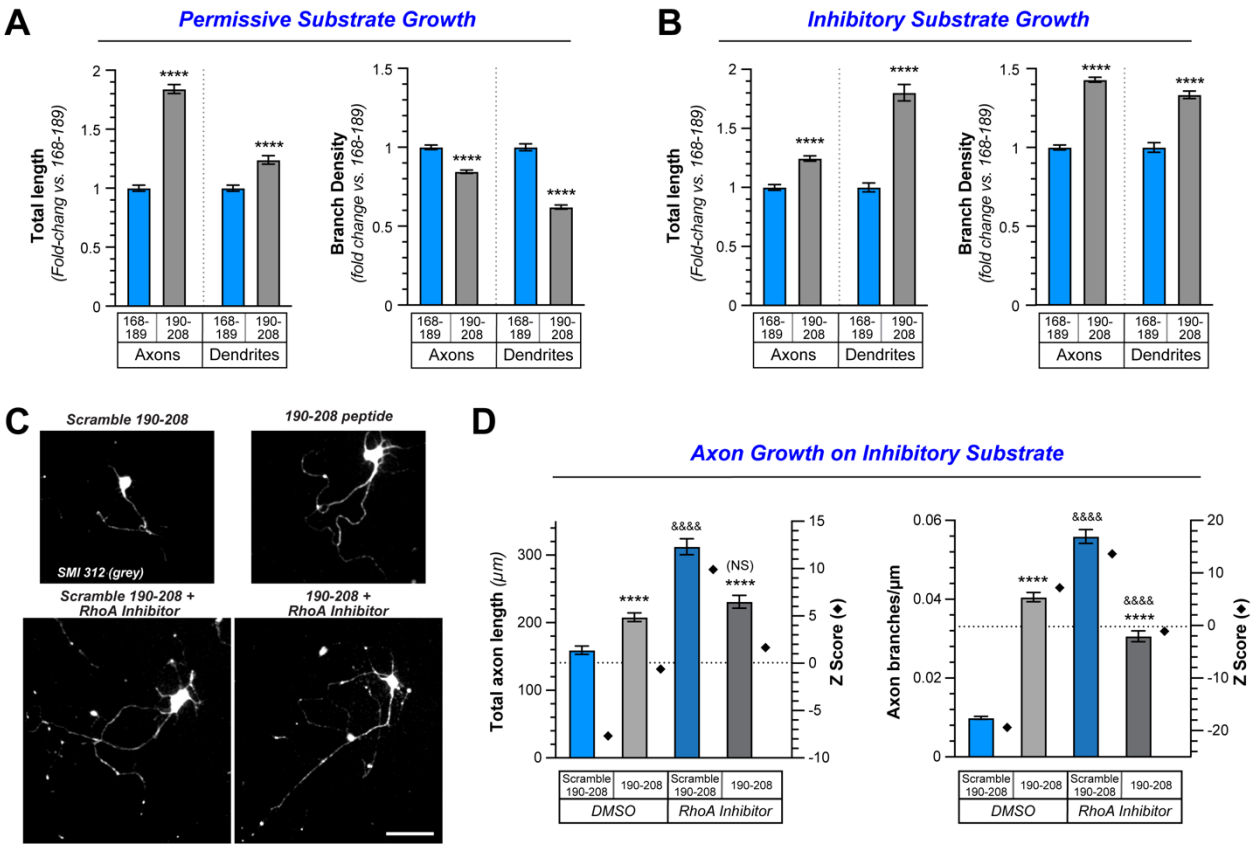
A
Permissive Substrate Growth
Total length
(Fold-chang vs. 168-189)
Branch Density
(fold change vs. 168-189)
168-189
190-208
Axons
Dendrites
B
Inhibitory Substrate Growth
C
Scramble 190-208
190-208 peptide
SMI 312 (grey)
Scramble 190-208 + RhoA Inhibitor
190-208 + RhoA Inhibitor
D
Axon Growth on Inhibitory Substrate
Total axon length (μm)
Axon branches/μm
Z Score (◆)
(NS)
DMSO
RhoA Inhibitor